Jurnal MIPA dan Pembelajarannya
e-issn: 2798-0634, email: jmipap.journal@um.ac.id

VOL	ISS	YEAR	DOI
6	1	2026	10.17977/um067.v6.i1.2026.5

LASER ABLATION SYNTHESIS AND CHARACTERIZATION OF GOLD-ZIRCONIUM OXIDE NANOPARTICLES

Ali Fadhil Abdulaali

Wasit General Directorate of Education, Wasit, Iraq
*Corresponding author, email: aliaa7648@gmail.com

Keywords
Pulsed Laser Ablation in Liquid
Au–ZrO_2 Nanocomposites
Gold Nanoparticles
Zirconium Oxide
Surface Plasmon Resonance
X-ray Diffraction

Abstract
The synthesis and characterization of gold-zirconium oxide (Au-ZrO_2) nanoparticles by Pulsed Laser Ablation in Liquid (PLAL) technique is presented. The stable colloidal suspensions of gold and zirconium nanoparticles were generated by ablation of targets made of high purity gold and zirconium, respectively, in deionized water at different laser energies. The obtained nanomaterials were deposited onto the substrates by drop-casting and then subjected to calcination to improve the crystallinity and bonding at the interface. UV–Vis spectroscopy was utilized to investigate the optical properties, which showed prominent surface plasmon resonance (SPR) peaks for Au nanoparticles and broad absorbance range characteristic of the ZrO_2 wide band gap. The crystallite size of the Au and ZrO_2 phases was determined to be ~ 14.2–14.4 nm, respectively, by X-ray diffraction (XRD) analysis, and the phases formed were found to be face-centered cubic (FCC) Au and cubic ZrO_2. The images obtained by Field Emission Scanning Electron Microscopy (FESEM) showed uniformity in morphology, the nanometric particle size and possibility of core–shell structures. Overall, the Au-ZrO_2 nanocomposites synthesized by PLAL demonstrate structural and optical properties suitable for various applications, including gas sensing, photocatalysis, and optoelectronics, highlighting the potential of PLAL for producing high-performance advanced nanomaterials.

1. Introduction

Nanostructured metal oxide semiconductors have remarkable properties, such as photo catalytic surfaces, gas sensors etc. (Wang et al., 2010; Franke et al., 2006) making them very versatile in applications. Over the last several years, low dimensional metal oxide nanowires and nanoribbons have emerged as a very popular class of nanowire structure in the realm of gas sensing. When these materials are reduced to dimensions of the order of 100 nanometers or less, quantum mechanical effects become significant and govern the properties of the material (Kelly et al., 2003; Jain et al., 2008). In this size range, many of the physical properties of the material, such as thermal, electrical, optical and mechanical properties change significantly from bulk properties. A major transformation is the tremendous increase in surface area to volume ratio which can significantly improve the thermal reactivity and catalytic performance. Also, as the size of the semiconductor metal oxide particles becomes comparable to the critical size (80-100 nm), the electrons start to be redistributed from the bulk donor states to the surface vacancies. This change results in a correspondingly large decrease by as much as three orders of magnitude in the bulk conduction electron density. Consequently, the electrical conductance of these nanomaterials is extremely responsive to the small variations in the concentration of the gas molecules adsorbed on their surface, making them suitable for use as gas sensors of future generation. Gas sensors are essential in many applications, including industrial gas analysis, scientific research and remote sensing, as well as in the protection of people and the environment (Korotcenkov, 2008; Wang et al., 2010). Some of the most important parameters they define are sensitivity, selectivity and long-term stability. A range of strategies have been employed to improve these sensing capabilities, especially their ability to strongly and selectively respond to specific gases. These include microstructural engineering, the addition of dopants or additives, physicochemical filtration and careful control of operating temperature. Nitrogen dioxide (NO_2) is one of the most harmful and monitored pollutants (Wang et al., 2010). This

noxious, reddish-brown gas is harmful to humans, animals, and the environment and has a strong smell. In addition, NO_2 is a vital component of air and water pollution, making its presence particularly relevant in applications like air quality assessment and monitoring wastewater treatment processes. There are different methods including doping, composite, nanoscale particle size, and high operation temperature of the semiconductor material to increase the sensitivity of semiconductor material to target gases. Porous silicon (PS), for one thing, has distinct physical and chemical attributes which set it apart from the familiar single crystal silicon. These special characteristics make it particularly desirable for gas sensing applications. The electrochemical etching process which is employed to produce PS forms a highly porous surface, with parts of the silicon crystal being selectively removed. This structural change allows for new physical properties like increased surface area and reactivity that benefits sensor performance. Another important n-type semiconductor material with interesting properties for optical and sensing applications is zirconium oxide (ZrO_2) (Guo, 2004; Chevalier, 2006). The crystalline structure and lattice defects give it a range of band gaps and high optical transmittance in the visible part of the solar spectrum. Moreover, ZrO_2 has great photocatalytic activity, which allows it to degrade harmful chemical compounds, dyes, pigments and environmental pollutants (Hagfeldt & Grätzel, 1995; Anpo & Takeuchi, 2003).

In this context, gold nanoparticles (Au NPs) are very promising candidates to be used on the gas sensing platforms. These surface plasmon resonance, chemical stability and synergistic action with other metal oxides such as ZrO_2 gives them high sensitivity, selectivity and performance for gas detection (Link & El-Sayed, 1999; Kelly et al., 2003; Jain et al., 2008).Transparent zirconium dioxide (ZrO_2) semiconductors have been extensively reported in the literature for gas sensing applications for a variety of gases. Gold nanoparticles (Au NPs) are highly attractive among the noble metals due to their exceptional physicochemical properties (Haruta, 1997; Kelly et al., 2003) that are strongly dependent on the particle size and shape. The properties of these include thermal stability, unique optical behaviour and non-toxicity, which would be suitable for several sensing applications. Optical properties of composite structures such as Au–ZrO_2 are strongly influenced by the size and the interparticle distance of the created nanomaterials. Their sensing performance and the overall material behavior is directly dependent on these structural parameters. In the case of Au:ZrO_2 nanocomposites, the pulsed laser ablation (PLA) technique in liquids is proven to be an effective method for their synthesis (Yang, 2007; Amendola & Meneghetti, 2009; Zhang et al., 2017). By this method, it is possible to control the formation of nanoparticles with some specific morphology and it is a very powerful method to develop advanced gas sensor materials. Another major advantage of this method is its simplicity, low cost, and cleanliness (Zhang et al., 2017; Theerthagiri et al., 2022), which means that it does not require complex vacuum systems, and will cause less contamination in the production of nanoparticles. The Pulsed Laser Ablation (PLA) method involves intense, short duration laser pulses (usually nanosecond in duration) from an infrared laser focused on a target material to produce nanoparticles with properties that differ at the nanoscale. A metallic target ablated in a liquid medium can experience partial oxidation which can lead to the creation of metal cations on the surface of the ablated nanoparticles. This oxidation is enhanced by the creation of ROS species at the plume–liquid interface (liquid plasma region) due to the breakdown of the surrounding liquid. This interaction between the laser, target and liquid enables PLA to be a powerful and versatile approach to the production of high purity nanomaterials with specific surface properties.

2. Materials and Methods

2.1 Synthesized

High-purity gold (Au) and zirconium (Zr) sheets (2 cm × 2 cm, 99.99%) were used to synthesize the metal nanoparticles. The experimental setup of pulsed laser ablation in liquid (PLAL) is shown in figure 1 (Yang, 2007; Zhang et al., 2017). The system comprises an Au/Zr target, which is flat, and is immersed in distilled deionized water (DDW) within a glass chamber, and an Nd:YAG laser. To obtain a uniform ablation, the Au target was placed on a rotating platform, at the bottom of the chamber, which had a 99.99% purity, and a thickness of 3 mm. A focusing lens guided the laser beam to the target, reducing the amount of localized overheating. To make gold nanoparticles, the target was irradiated with 200 laser pulses (λ = 1064 nm, 6 Hz frequency) at different energies (50-200 mJ), the laser being 12 cm above the target. DDW was used as the ablation medium and a volume of 5 mL was used. This process yielded a stable purple gold nanoparticles' colloid within the DDW. The same laser ablation technique was used to produce Au-ZrO_2 nanocomposites by ablation of the Zr target in the pre-synthesized gold colloid. The laser energy caused simultaneous ablation of Zr and fragmentation of the existing gold nanoparticles, leading to formation of hybrid Au-ZrO_2 nanostructures. The idea

is to use the liquid environment to stabilize the nanoparticles and to avoid aggregation (Amendola & Meneghetti, 2009).

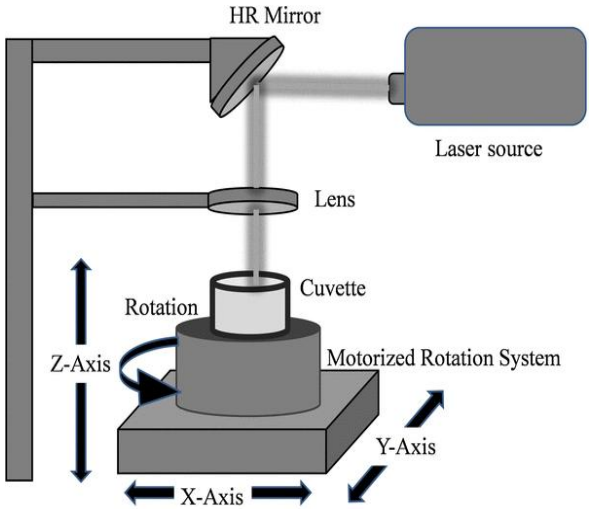

Figure 1 .Schematic diagram of the experimental set-up for the synthesis of Au, ZrO2 nanoparticles by laser ablation method

2.2 Drop-casting technique

The colloidal solutions of the nanoparticles were then utilized to prepare thin films using drop casting method after the synthesis. This method involved the careful application of measured volumes of the colloidal solution on the clean glass or quartz substrates with a micropipette. The solid substrates were then allowed to remain on a hotplate at 80-90C to slowly dry the solvent (DDW). This was a controlled drying process, which helped nanoparticles to be uniformly deposited on the surface of the substrate. The drop-casting was repeated in a few cycles to obtain a thicker and more uniform film, drying the layers between drop-casts to crystallize in order to enhance the uniformity of the film. The method provided good adhesion, full coverage of the substrate surface and uniform distribution of the nanoparticles, and the resulting films were ideal for structural, optical and sensing applications (Routh, 2013; Brinker & Scherer, 1990).

2.3 Post-deposition calcination

After that, the fabricated films were treated with a calcination process to enhance the structural and functional properties of the films. The samples were then put into a furnace and heated at 400°C for 1 hour in ambient air. This thermal treatment was used for a number of reasons:

- Crystallization enhancement: Improvement of the crystalline structure of ZrO_2 and Au-ZrO_2, reduction of lattice defect.
- Phase stabilization: Stable tetragonal or monoclinic phase of ZrO_2 was obtained.
- Interfacial bonding: Promoted strong bonding between Au and ZrO_2 nanoparticles, which is crucial for enhanced electron transport in sensing and catalytic applications.

Remove Organic Residues: None of the organic residues were left behind from the synthesis or deposition process.

The integration of PLAL, drop-casting, and post-deposition calcination enabled the fabrication of high-quality Au–ZrO_2 nanostructured thin films with controlled morphology, improved crystallinity, and enhanced functional performance (Theerthagiri et al., 2022).

3. Result and Discussion

UV–Vis spectroscopy was used to examine the absorbance spectrum of Au nanoparticles produced with different laser energies (50, 100, 150, 200 and 250 mJ) at 1064 nm wavelength. The measurements were carried out in the wavelength range of 200 nm to 250 nm, with deionized distilled water as the reference medium in a quartz cuvette. This is the absorbance spectrum of Au NPs prepared under various laser pulse energies as shown in Figure 2 (a).

The absorbance spectra display a characteristic surface plasmon resonance (SPR) peak in the range of 520 nm to 560 nm, which is a well-known optical property of Au NPs (Link & El-Sayed, 1999; Kelly et al., 2003). The most prominent SPR peak is found at 150 mW, suggesting an optimum energy level for the production of nanoparticles. The absorbance in this energy is more than 1.6, which shows a high concentration of well-dispersed nanoparticles which are in the best size and shape to be plasmonic. The SPR peaks at lower energies (50 and 100 mJ) are less intense and slightly red-shifted, presumably because the particles are larger or less regular, or have wider size distributions. The absorbance rises at the higher energies (200 and 250 mJ), but does not exceed the absorbance at 150 mJ. This may be because of secondary fragmentation or agglomeration effects which lead to less uniformity of nanoparticles. The tailing of the absorbance curves beyond 700 nm suggests wider particle size distributions and/or interparticle interactions at higher concentrations. From the above figures it is clear that the laser energy used in the synthesis of nanoparticles has a significant impact on the absorbance. The sample irradiated with 100 mJ showed the highest absorbance (~0.75) in the UV region (200-225 nm) suggesting that there was a higher concentration of nanoparticles or more effective nanoparticles formation at this energy. A gradual decrease in absorbance was seen with increasing laser energy (150 mJ, 200 mJ and 250 mJ), indicating a change in particle size, crystallinity or particle concentration. This may be explained by the breakup of particles at higher energies and/or by the lower production of less optically active species because of the plasma shielding effect. Absorbance of all the samples lies within the range of about 200 nm to 480 nm, and it is found that absorbance is maximum in the UV region, which is characteristic of wide band gap nature of ZrO_2. This large-bandwidth of absorbance makes it useful for optoelectronic and gas sensing applications. The absorbance dependency on particle size attributed to the PLA energy, suggests quantum confinement effects (Jain et al., 2008). The smaller the nanoparticles (usually generated at moderate energies such as 100mJ) the more intense the absorbance, which arises from having a higher surface area-to-volume ratio, and electronic transitions in the band structure of the material.

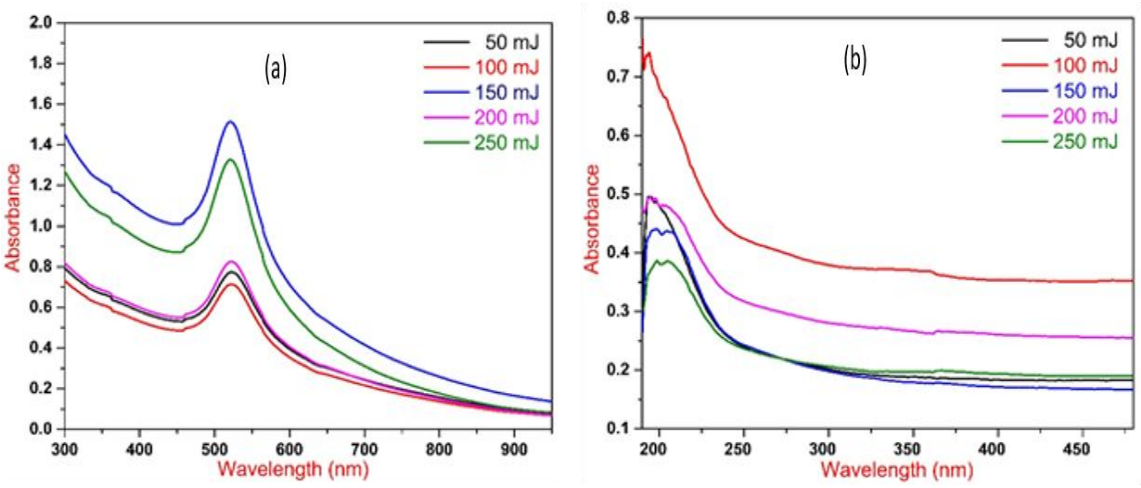

Figure 2. UV-Visible absorbance of (a) Gold NPs, (b) Zirconium oxide NPs NPs, in different laser energies

Gold nanoparticles (Au NPs) were prepared by the laser ablation method. The X-ray diffraction (XRD) pattern obtained for the resultant particles showed four sharp peaks, at 2θ angles of 38.43°, 44.73°, 65.23° and 78.33° which indicated the presence of pure gold nanoparticles (Figure 3). The peaks correspond to crystallographic planes (111), (200), (220) and (311) characteristic of the face-centered cubic (FCC) structure of gold with JCPDS card No. 96-901-1613 as shown in Figure 3. The average crystallite size was calculated using the Scherrer equation:

$$D = \frac{K\lambda}{\beta \cos \theta_B}$$

where D is the crystallite size, K is the shape factor, λ is the X-ray wavelength, β is the full width at half maximum (FWHM), and θB is the Bragg angle (Gesing et al., 2024).

The mean size of the Au NPs synthesized was estimated to be about 14.4 nm. The detailed peak positions, the indices of the planes along which the diffraction occurred and the value of the full width at half maximum (FWHM) are 0.65 (Scherrer, 1918; Patterson, 1939). The X-ray diffraction (XRD)

pattern of the synthesized Au-ZrO_2 nanoparticles displays eight distinct peaks at 2θ values of 30.05°, 35.51°, 37.95°, 44.15°, 50.1°, 59.8°, 64.4°, and 77.35°, as shown in Figure 3. These peaks correspond to the crystallographic planes (Miller indices) of (111), (200), (111), (200), (220), and (311), respectively. Of these, the diffraction peaks for 37.95°, 44.15°, 64.4° and 77.35° are assigned to diffraction from pure gold nanoparticles, which is close to the face-centered cubic (FCC) structure of gold (Haruta, 1997). The peaks at 30.05°, 35.51°, 50.1° and 59.8° are attributed to the cubic structure of the ZrO_2 nanoparticles (Chevalier, 2006). The average crystallite size of Au-ZrO_2 nanoparticles was determined by the Scherrer equation from the full width at half maximum (FWHM) and 2θ values of Au and ZrO_2 diffraction peaks and was found to be around 14.2 nm (Gesing et al., 2024).

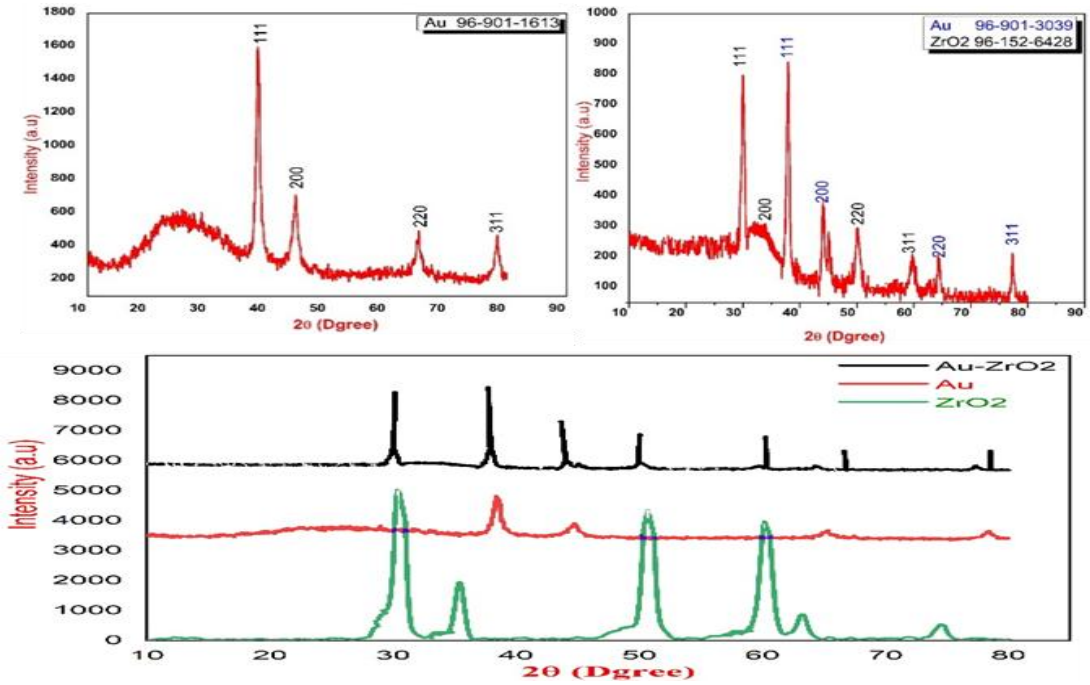

Figure 3. XRD patterns of Au, ZrO2 Au-ZrO2 and Au thin film prepared by PLA

The images of nanoparticles prepared by Pulsed Laser Ablation in Liquids (PLAL) process method of Au, ZrO_2, hybridized nanoparticles of Au-ZrO_2, and core/shell nanoparticles of Au-ZrO_2 are shown in Figure 4. Images were captured at various magnifications to gain information about the surface morphology, size and crystallographic texture of the generated nanomaterials. The high magnification image on the left (330,000X; scale bar of 100 nm) shows the near-spherical shaped nanoparticles as densely packed, uniform grains. It is a structure typical of pure Au or Au-rich particles, and it is the result of the exact control of the particle size and shape that has been obtained by the PLAL technique (Amendola & Meneghetti, 2009; Zhang et al., 2017). The texture is smooth and the size distribution narrow indicating high crystallinity and absence of aggregation, a desirable property for catalysis, plasmonic sensing (Primo et al., 2011), etc. The image on the right (100,000x; 500nm scale bar) shows a more complex surface topography with larger spherical structures being rough-surfaced, with smaller particulates surrounding them. These features suggest the presence of ZrO_2-enriched areas or core–shell structures having gold cores surrounded by a shell of ZrO_2. Metal oxides such as ZrO_2 are often found with flower-like or cauliflower morphology that is beneficial for photocatalytic and electrochemical applications (Chevalier, 2006; Anpo & Takeuchi, 2003). In the two images, the differences in structure and hierarchical assembly are highlighted by PLAL synthesis. This approach can be used for the production of specially designed nanocomposites having controlled morphology that is crucial in optimizing the performance of the material for different applications in nanotechnological and energy-related applications (Theerthagiri et al., 2022).

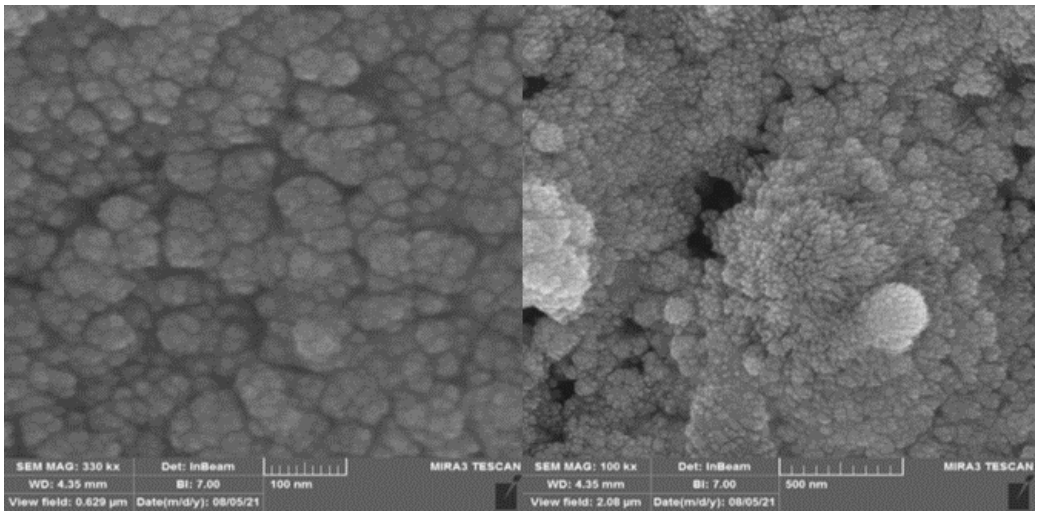

Figure 4. FE-SEM image of Au and morphology of nanoparticles

The FESEM image of the ZrO_2 nanoparticles obtained by Pulsed Laser Ablation in Liquids (PLAL) at two magnifications is shown in Figure 5: 100,000× shown on left, 330,000× shown on right. The ZrO_2 nanoparticles show a more clustered structure at lower magnification (left, 500 nm scale bar), characterized by the presence of spherical and cauliflower-like aggregates. The morphology indicates that the surface is rough and porous, and is a common feature of laser-ablated zirconia (Yang, 2007; Theerthagiri et al., 2022). Rough surface features are beneficial for applications like photocatalysis and electrochemical sensors because they increase the active surface area (Anpo & Takeuchi, 2003; Chevalier, 2006). The high magnification image (right, 100 nm scale bar) shows greater detail of the fine nano-grains which make up the larger structures. The individual particles seem to be almost spherical and are closely packed together, suggesting that homogeneous nucleation and growth occurred during the process of laser ablation (Amendola & Meneghetti, 2009). The uniformity and compactness of these nanoparticles indicate high crystallinity of the zirconia, which is in accordance with the high stability and structural strength of zirconia (Guo, 2004; Chevalier, 2006).

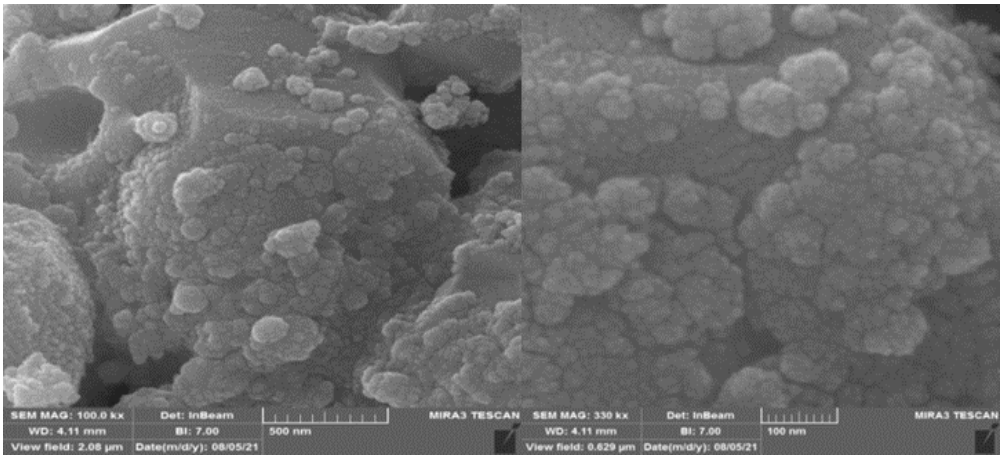

Figure 5. FE-SEM image of ZrO2and morphology of nanoparticles

Figure 6 shows the Field Emission Scanning Electron Microscopy (FESEM) images of Au-ZrO_2 nanocomposite prepared by Pulsed Laser Ablation in Liquids (PLAL) technique, which exhibits morphological characteristics associated to the formation of hybrid nanoparticles.

3.1 Morphological Observations

Nanoparticle Distribution: The FESEM images show a uniform distribution of nanoparticles, ranging in size between about 50 to 100 nm. This is the range of sizes in which nanostructured materials can be formed for a wide range of applications.

Surface Texture: The surface texture of the nanoparticles is relatively smooth, indicating good crystallinity and purity. These properties are desired in applications that need uniformity in surface properties (Primo et al., 2011).

Core–Shell Structures: Some particles exhibit contrast differences that could be suggestive of core–shell structures that involve gold cores surrounded by shells of zirconia. This structural configuration can be beneficial to increase the stability and catalytic activity of the nanoparticles (Primo et al., 2011; Haruta, 1997).

3.2 Nano-Analytical Insights

The observed morphologies are consistent with the known crystalline structures of Au and ZrO_2, which indicates successful synthesis of the desired nanocomposite (Chevalier, 2006; Haruta, 1997).

Synthesis Efficacy: The uniformity and distinct features observed confirms the efficacy of the PLAL in the creation of high-quality Au-ZrO_2 nanocomposites (Zhang et al., 2017; Theerthagiri et al., 2022).

These characteristics highlight the potential applications of the Au-ZrO_2 nanocomposites in catalysis, sensing, and other areas that demand high surface area and stability (Primo et al., 2011; Theerthagiri et al., 2022).

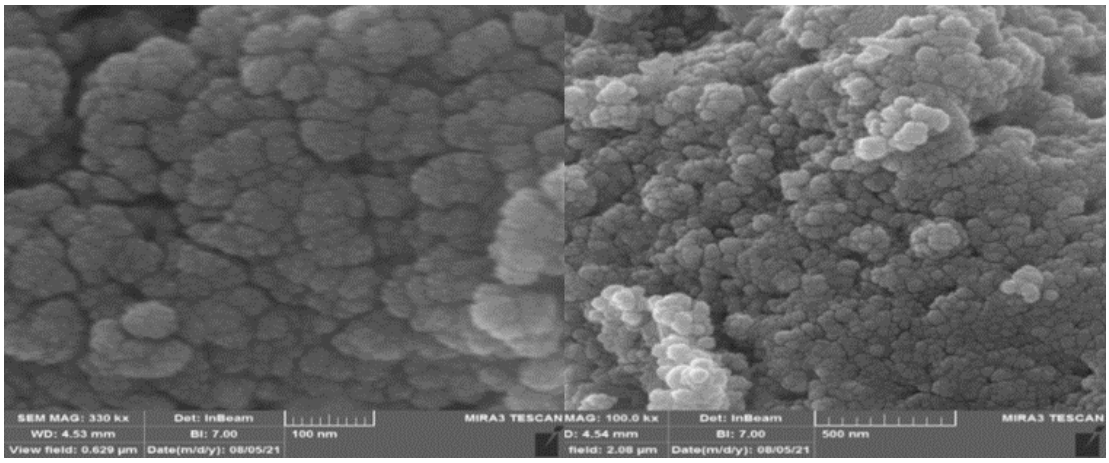

Figure 6. FE-SEM image of Au-ZrO2 and morphology of nanoparticles

4. Conclusion

The synthesis and characterization of gold-zirconium oxide (Au-ZrO_2) nanocomposites by pulsed laser ablation in liquid (PLAL) technique have been successfully achieved. The laser ablation, drop casting and post-deposition calcination method were successfully applied for preparation of nanostructured films having controlled morphology and crystallinity. The well-dispersed Au nanoparticles were confirmed by UV–Vis spectroscopy, which showed sharp surface plasmon resonance peaks with the best nanoparticle generation at 150 mJ laser energy. The analyses by X-ray diffraction (XRD) validated the formation of the desired nanocomposites and confirmed the characteristic peaks of both Au and ZrO_2, with an average crystallite size of about 14.2–14.4 nm estimated. The synthesized nanomaterials were also characterized by Field Emission Scanning Electron Microscopy (FESEM) to show a uniform morphology, particle size distribution and possible core–shell structures.

The nanocomposites based on Au and ZrO_2 combine the gas-sensing properties of Au with semiconducting and photocatalytic properties of ZrO_2, which enables the development of nanocomposites with gas-sensing, photocatalytic and optoelectronic applications (Haruta, 1997; Anpo & Takeuchi, 2003; Chevalier, 2006). The structural and optical properties observed suggest PLAL as an efficient and clean technique to obtain the high quality hybrid nanomaterials with tunable properties (Theerthagiri et al., 2022; Zhang et al., 2017). Future studies could include detailed gas sensing evaluations, long-term stability studies and the extension of the scope of synthesis to other metal–oxide systems for wider application areas.

References

Amendola, V., & Meneghetti, M. (2009). Laser ablation synthesis in solution and size manipulation of noble metal nanoparticles. *Physical Chemistry Chemical Physics, 11*(20), 3805–3821. https://doi.org/10.1039/B900654K

Anpo, M., & Takeuchi, M. (2003). The design and development of highly reactive titanium oxide photocatalysts. *Journal of Catalysis, 216*(1–2), 505–516. https://doi.org/10.1016/S0021-9517(02)00104-5

Brinker, C. J., & Scherer, G. W. (1990). *Sol–gel science: The physics and chemistry of sol–gel processing*. Academic Press.

Chevalier, J. (2006). What future for zirconia as a biomaterial? *Biomaterials, 27*(4), 535–543. https://doi.org/10.1016/j.biomaterials.2005.07.034

Franke, M. E., Koplin, T. J., & Simon, U. (2006). Metal and metal oxide nanoparticles in chemiresistors. *Small, 2*(1), 36–50. https://doi.org/10.1002/smll.200500261

Gesing, T. M., et al. (2024). Determination of the average crystallite size and the consequences for materials characterization. *Journal of Applied Crystallography, 57*(5).

Guo, X. (2004). Property degradation of tetragonal zirconia induced by low-temperature defect reaction. *Chemistry of Materials, 16*(21), 3988–3994. https://doi.org/10.1021/cm049560f

Hagfeldt, A., & Grätzel, M. (1995). Light-induced redox reactions in nanocrystalline systems. *Chemical Reviews, 95*(1), 49–68. https://doi.org/10.1021/cr00033a003

Haruta, M. (1997). Size- and support-dependency in the catalysis of gold. *Catalysis Today, 36*(1), 153–166. https://doi.org/10.1016/S0920-5861(96)00208-8

Jain, P. K., Huang, X., El-Sayed, I. H., & El-Sayed, M. A. (2008). Review of some interesting surface plasmon resonance-enhanced properties of noble metal nanoparticles. *Accounts of Chemical Research, 41*(12), 1578–1586. https://doi.org/10.1021/ar7002804

Kelly, K. L., Coronado, E., Zhao, L. L., & Schatz, G. C. (2003). The optical properties of metal nanoparticles: The influence of size, shape, and dielectric environment. *The Journal of Physical Chemistry B, 107*(3), 668–677. https://doi.org/10.1021/jp026731y

Korotcenkov, G. (2008). Metal oxides for solid-state gas sensors: What determines our choice? *Materials Science and Engineering: B, 139*(1), 1–23. https://doi.org/10.1016/j.mseb.2007.01.044

Link, S., & El-Sayed, M. A. (1999). Size and temperature dependence of the plasmon absorption of colloidal gold nanoparticles. *The Journal of Physical Chemistry B, 103*(21), 4212–4217. https://doi.org/10.1021/jp984796o

Mat Isa, S. Z., Zainon, R., & Tamal, M. (2022). State of the art in gold nanoparticle synthesisation via pulsed laser ablation in liquid and its characterisation for molecular imaging: A review. *Materials, 15*(3), Article 875. https://doi.org/10.3390/ma15030875

Primo, A., Corma, A., & García, H. (2011). Titania supported gold nanoparticles as photocatalyst. *Physical Chemistry Chemical Physics, 13*(3), 886–910. https://doi.org/10.1039/C0CP00917B

Routh, A. F. (2013). Drying of thin colloidal films. *Reports on Progress in Physics, 76*(4), Article 046603. https://doi.org/10.1088/0034-4885/76/4/046603

Theerthagiri, J., et al. (2022). Fundamentals and comprehensive insights on pulsed laser synthesis of advanced materials for energy and environmental applications. *Light: Science & Applications, 11*, Article 250. https://doi.org/10.1038/s41377-022-00904-7

Trovarelli, A. (1996). Catalytic properties of ceria and CeO_2-containing materials. *Catalysis Reviews, 38*(4), 439–520. https://doi.org/10.1080/01614949608006464

Wang, C., Yin, L., Zhang, L., Xiang, D., & Gao, R. (2010). Metal oxide gas sensors: Sensitivity and influencing factors. *Sensors, 10*(3), 2088–2106. https://doi.org/10.3390/s100302088

Yang, G. W. (2007). Laser ablation in liquids: Applications in the synthesis of nanocrystals. *Progress in Materials Science, 52*(4), 648–698. https://doi.org/10.1016/j.pmatsci.2006.10.016

Zhang, D., Gökce, B., & Barcikowski, S. (2017). Laser synthesis and processing of colloids: Fundamentals and applications. *Chemical Reviews, 117*(5), 3990–4103. https://doi.org/10.1021/acs.chemrev.6b00468